International Forum on Aeroelasticity and Structural Dynamics
IFASD 2024
17-21 June 2024, The Hague, The Netherlands

INFLUENCE OF CRUISE ALTITUDE VARIATION ON THE TURBULENCE LOADS OF A MEDIUM-RANGE TRANSPORT CONFIGURATION

Vega Handojo[1*], Sunpeth Cumnuantip[1]

[1] DLR – Institute of Aeroelasticity, Bunsenstr. 10, 37073 Göttingen, Germany
[*]vega.handojo@dlr.de

Keywords: flight loads, continuous turbulence, load collectives, altitude variation

Abstract: For the cruise condition of transport aircraft, variations in the cruise altitude prove to be a promising way to reduce the generation of persistent condensation trails and their thermodynamic effects on the environment. At varied altitudes, however, the expected atmospheric turbulences and thus the loads acting on the aircraft might be different. In this work, the research question regarding the turbulence loads at varied altitudes is addressed. For that aim, a medium-range transport configuration is taken as reference. Subsequently, a method to calculate turbulence loads in the frequency domain is applied, and the transform into the time domain as well as the derivation of load collectives using the rainflow-counting method are explained. Results show that the largest fraction of variations in the loads and vertical accelerations emerge through the change in the turbulence intensities which are a function of the altitude. Beyond that, slight variations in the aircraft's dynamic responses among the altitudes are observable.

1 INTRODUCTION

In the past decades, there have been various innovations to minimize the environmental footprint of aviation. Recent research showed that the climate impact of flight operation not only lies in the CO2 emission, but also in the thermodynamic effects of persistent condensation trails [1][2]. The latter might emerge when an aircraft flies through ice-supersaturated air [2], so that the water vapor from the engine exhaust – which turns into ice – cannot be contained by the air anymore.

For a flying aircraft, one possible method to mitigate the thermodynamic effects of persistent condensation trails is by reducing or raising the cruise altitude, depending on the atmospheric conditions [3][4]. At varied altitudes, however, the expected atmospheric turbulence intensities are different [5], and combined with the possible necessity to vary the flight speed, the loads acting on the aircraft might be different. At this point, the research question emerges: How do the turbulence loads change if the cruise altitude is varied?

To answer that question, the following steps are carried out: Firstly, a medium-range configuration that is taken as the reference aircraft is outlined, followed by its aeroelastic modeling. Secondly, a method to calculate turbulence loads in the frequency domain including the transform into the time domain is elaborated. Moreover, a rainflow-counting method that is used to derive load collectives from the time domain turbulence responses is explained. The selected parameters used in the load calculations as well as the related considerations are elaborated as well.

2 REFERENCE AIRCRAFT AND ITS AEROELASTIC MODELS

For the turbulence load calculation, the mid-range configuration DLR-F25 [6] is taken as reference. The aircraft's main characteristics are its high aspect ratio wing (wing aspect ratio higher than 15), its novel wing movables configuration and its sustainable aviation fuel high bypass ratio engine. Table 1 lists a few key parameters of the aircraft.

Table 1. Key parameters of the DLR-F25 configuration

Parameter	**Value**
Wing span	45 m
Maximum zero-fuel mass	72000 kg
Maximum landing mass	74800 kg
Maximum take-off mass	86000 kg
(Economic) cruise Mach number	Mach 0.78
Maximum operating speed, Mach number	180 m/s EAS, Mach 0.82
Service ceiling	12192 m (40000 ft)

The aeroelastic simulation models for MSC.Nastran are created and optimized using the DLR in-house cpacs-MONA process [7]. The structure of the lifting surfaces is modelled with shell elements and the fuselage is represented by beam elements. Figure 1 visualizes the FE model of the DLR-F25; the shell elements on the fuselage and engine cowlings are for illustrational purpose only.

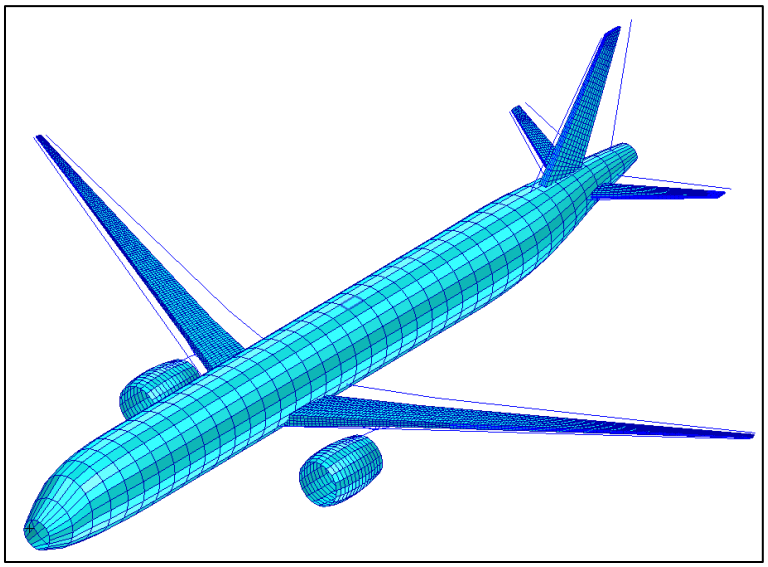

Figure 1. Global FE model of the DLR-F25

The aerodynamic forces are modelled based on the potential theory, namely using the vortex lattice method (VLM, for the quasi-steady cases) and doublet lattice method (DLM, for the dynamic cases) within MSC.Nastran [8]. Moreover, a slender body element and a corresponding set of interfering lifting surfaces are created to take the aerodynamic effect of the fuselage into account [9]. For the lifting surfaces, a twist and camber correction is considered, which evoke non-zero lift and pitch moment at zero angle of attack. Figure 2 shows the aerodynamic model of the DLR-F25 including the slender body for its fuselage.

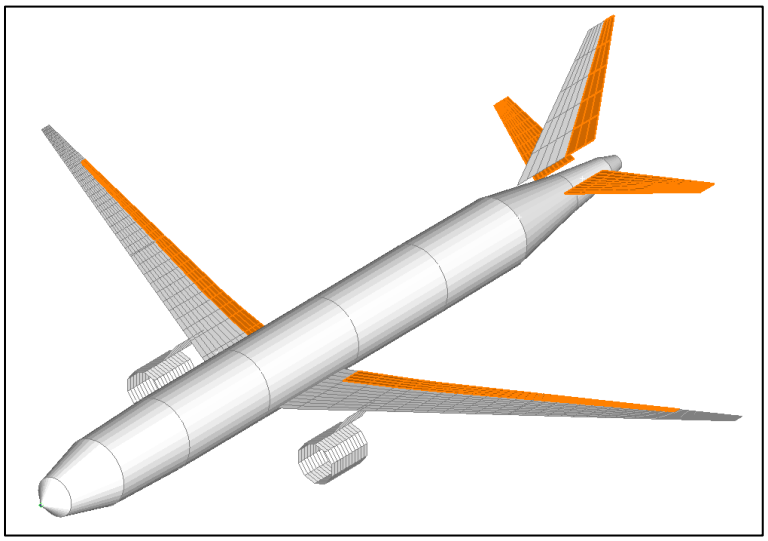

Figure 2. Aerodynamic model of the DLR-F25

3 TURBULENCE LOAD CALCULATION

To calculate the turbulence responses of an aircraft in a given flight condition, a turbulence spectrum as well as transfer functions of observed quantities of the aircraft are necessary. Both are generated / calculated in the frequency domain, and so are the resulting aircraft responses. Subsequently, the latter are transformed into the time domain, and a rainflow-counting algorithm is applied to derive the load collectives. Each aspect is elaborated in the following subsections based on [10].

3.1 Reference atmospheric turbulence

For the atmospheric turbulence, it is practical to consider the von Kármán spectrum since it is defined in the frequency domain already. It is also the spectrum prescribed in CS25.341(b)(2) [11]. The selected scale of turbulence is 762 m (2500 ft) as given in CS25. If formulated as a function of the frequency, the power spectral density (PSD) of the von Kármán spectrum is defined by:

$$\Phi(f)=\mathrm{rms}_w^2\,\frac{2L_{turb}}{V_{TAS}}\,\frac{1+\frac{8}{3}\left(1.339\cdot 2\pi f\frac{L_{turb}}{V_{TAS}}\right)^2}{\left(1+\left(1.339\cdot 2\pi f\frac{L_{turb}}{V_{TAS}}\right)^2\right)^{11/6}}, \tag{1}$$

with:

$\Phi(f)$: turbulence power spectral density [m²/s²/Hz],
rms_w^2 : root mean square of the vertical wind speed [m/s],
L_{turb} : scale of turbulence [m],
V_{TAS} : aircraft true airspeed [m/s]
f : frequency [Hz].

Figure 3 shows an exemplary PSD of the von Kármán spectrum with a root mean square (RMS) of the vertical wind speed of 1.0 m/s, a scale of turbulence of 762 m and a true airspeed of 231.3 m/s.

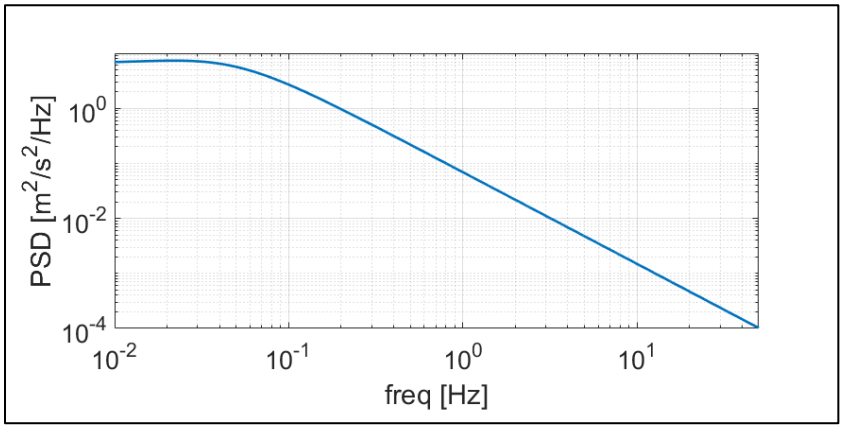

Figure 3. Exemplary von Kármán power spectral density

For each investiagted flight condition, a root mean square of the vertical wind speed is selected based on Figure 4 which is taken from MIL-STD-1797A [5]. For the load calculations, moderate turbulence intensities are assumed, which correspond to a probability of exceedance of the RMS of approx. 10^{-3}.

The vertical wind speed in the frequency domain is obtained by calculating the square root of the reference PSD and assigning a random phase angle (between 0 and 2π) for each frequency step. The vertical wind speed is calculated by:

$$w_{g,turb}(f) = \sqrt{\Phi(f) \cdot f_{max} \cdot 2n_f} \cdot e^{i \cdot rand(\varphi(f))}, \quad (1)$$

with:

$w_{g,turb}$: vertical wind speed [m/s],
n_f : number of elements in the frequency vector,
$rand(\varphi(f))$: random phase angle [rad].

Subsequently, $w_{g,turb}(f)$ is adjoined with its flipped complex conjugate to obtain its two-sided Fourier transform. Furthermore, the phase distribution $rand(\varphi(f))$ is set equal for every observed flight condition to minimize uncertainties due to statistical factors.

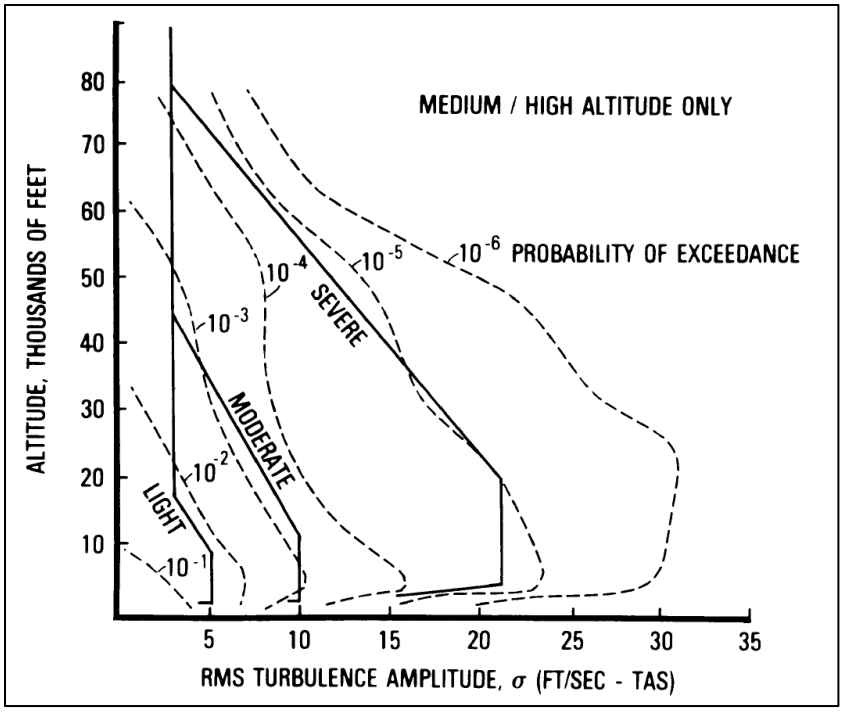

Figure 4. Probabilities of exceedance of various turbulence RMS [5]

3.2 Calculation of transfer functions

For every given flight condition, the transfer functions used for the turbulence loads analysis are calculated in the frequency domain using the dynamic aeroelastic solution sequence SOL 146 of MSC.Nastran [8]. The corresponding equations of motions are defined by:

$$[-M_{hh}\omega^2+iB_{hh}\omega+K_{hh}-\bar{q}Q_{hh}(Ma,k)]\{u_h\}=\{P_h(\omega)\}, \quad (2)$$

with:

M_{hh}	: modal mass matrix,
$\omega=2\pi f$	: circular frequency in rad/s,
B_{hh}	: modal damping matrix,
K_{hh}	: modal stiffness matrix,
$\bar{q}$	: dynamic pressure in Pa,
Q_{hh}	: aerodynamic matrix,
Ma	: Mach number,
k	: reduced frequency,
u_h	: modal displacements,
P_h	: generalized applied loads.

Since transfer functions are single input single output (SISO) systems, one transfer function is necessary for every combination of input and output quantities. In this case, the input is unit vertical wind speed and the outputs are cut loads at the wing root and approx. 55% half-span as well as vertical accelerations in the fuselage.

In the dynamic calculations with MSC.Nastran, the highest considered frequency is 50 Hz. According to the Nyquist-Shannon sampling theorem [12], this corresponds with a maximum time increment of 10 ms. To generate statistically relevant load collectives, 10^6 time steps are seen as

reasonable. The time increment multiplied with the number of time steps yields an observed time period of 10 000 s and a frequency increment of 10^{-4} Hz.

Figure 5 shows an exemplary transfer function of the bending moment response at the wing root to vertical wind speed. A slight peak of the short period mode is visible at approx. 0.25 Hz, and a more distinct peak of the first wing bending mode is found at approx. 2.6 Hz.

Analogous to the vertical wind speed, the transfer functions are then adjoined with their flipped complex conjugate form to obtain the two-sided form.

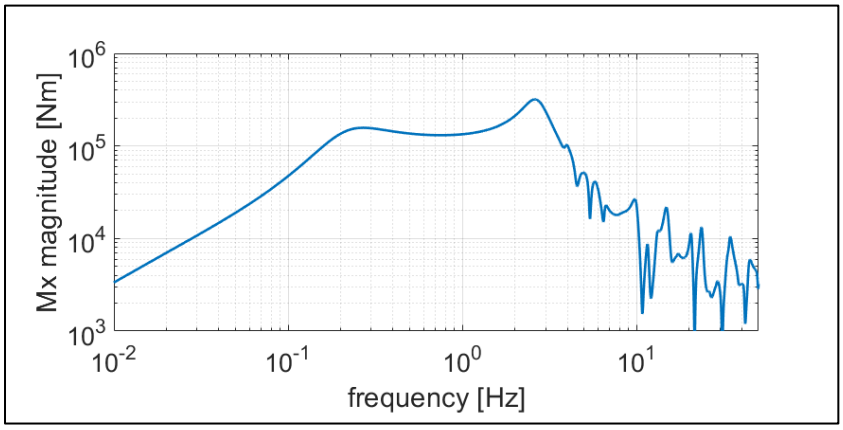

Figure 5. Exemplary transfer function of the wing root bending moment

3.3 Calculation of aircraft responses

In the frequency domain, the aircraft responses x(f) are calculated with an element-by-element multiplication of the (two-sided) vertical wind speed $w_{g,turb}(f)$ and the corresponding transfer functions $TF_{wg,turb\rightarrow x}(f)$:

$$x(f) = w_{g,turb}(f) \cdot TF_{wg,turb\rightarrow x}(f), \tag{3}$$

The responses x(f) are then transformed into the time domain for further analysis.

3.4 Calculation of load collectives

To obtain load collectives from the aircraft responses in continuous turbulence, a rainflow-counting algorithm [13] is applied. The steps are as follows:

- The time history of e.g. a response quantity is reduced to the local maxima and minima, see Figure 6.
- The graph is then rotated 90° clockwise and imagined as a pagoda roof.
- For the left side, each local maximum is imagined as a source of raindrops that start to flow. For the right side, the raindrops emerge at the local minima, see Figure 7.

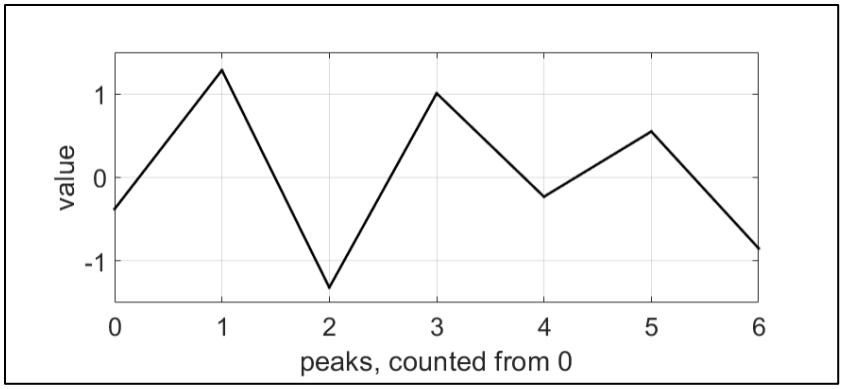

Figure 6. Exemplary peaks of a time history

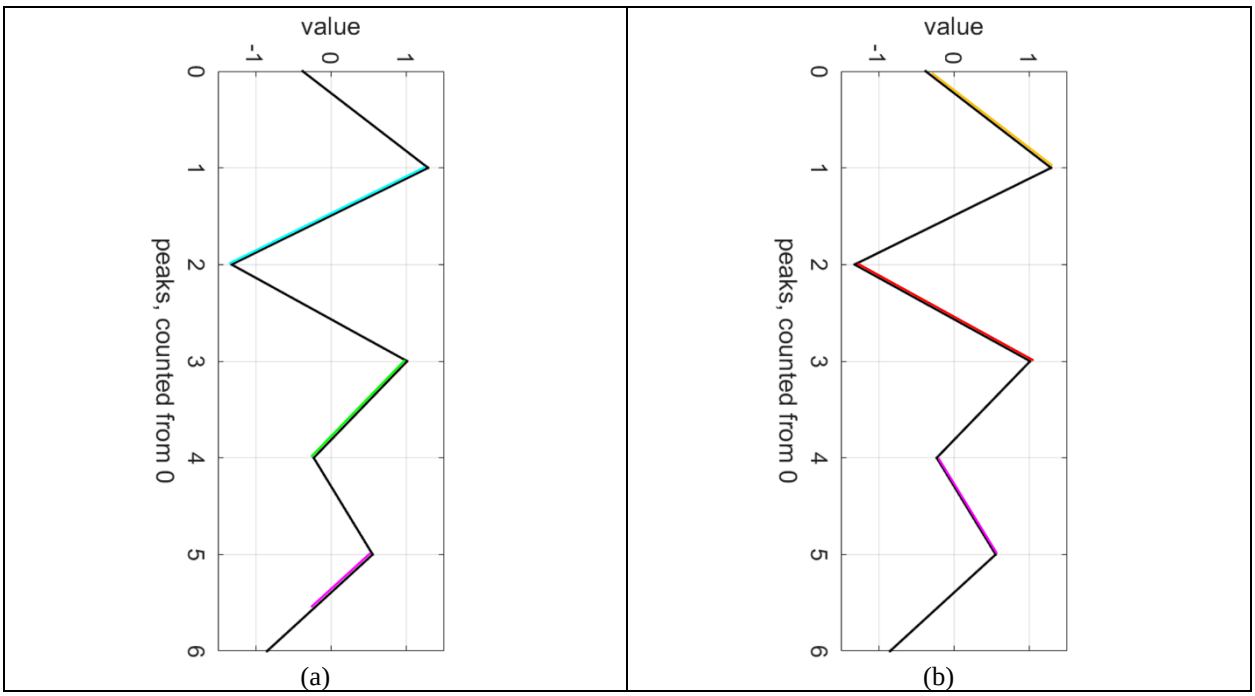

Figure 7. Raindrops appearing on the left (a) and right (b) side of the pagoda roof

- Each rainflow is continued, and it stops if either:
  - it reaches the end of the time history,
  - it merges with a flow that started at an earlier peak, or
  - the next raindrop source has a higher value (for the left side) or a lower value (for the right side), see Figure 8.

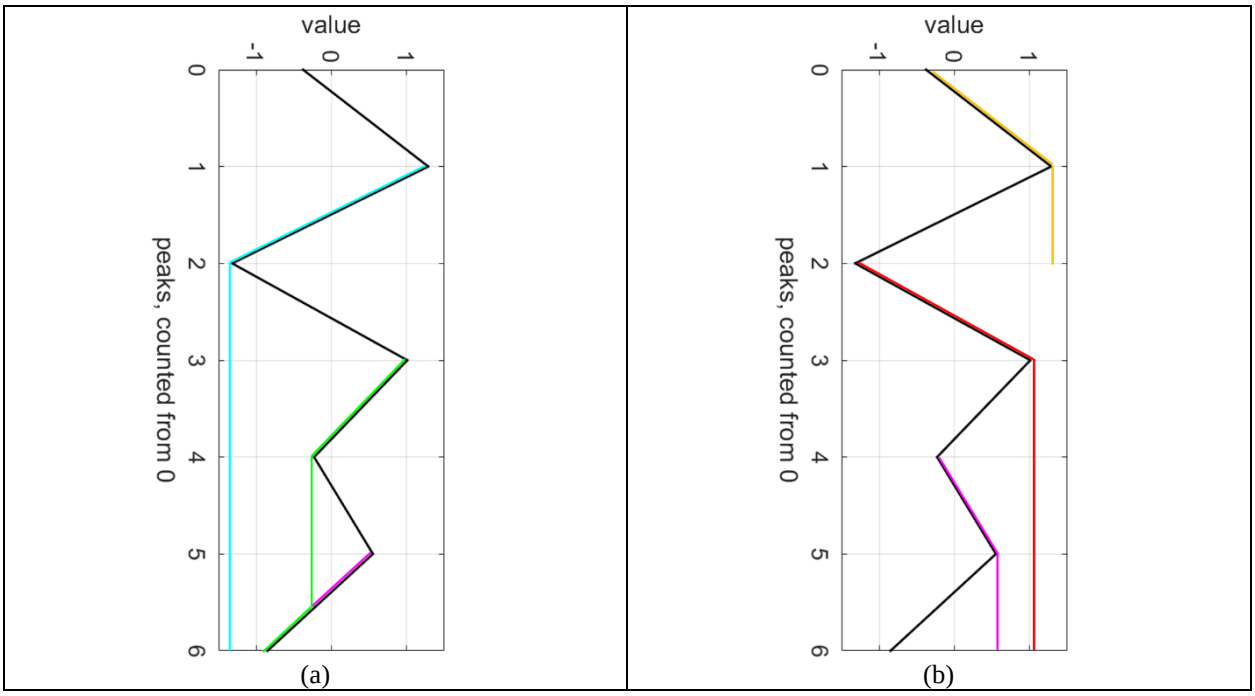

Figure 8. Rainflow continuation on the left (a) and right (b) side of the pagoda roof

- Each rainflow is counted as a half loading cycle. Half-cycles with the same magnitude are grouped together. In this case, half-cycles with the same color from the left and right side form a full cycle, see Figure 9.

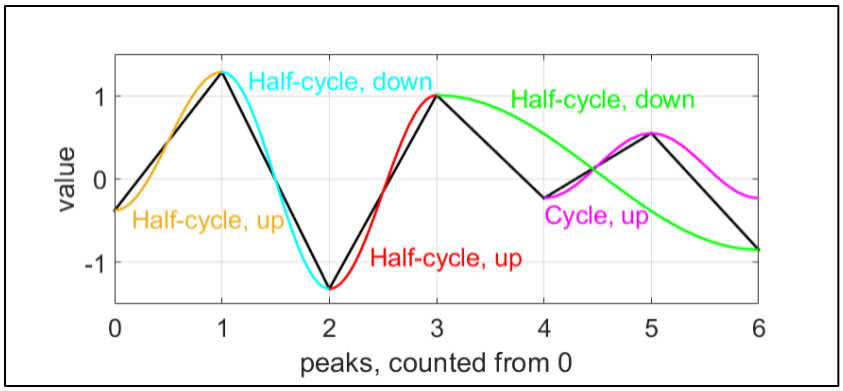

Figure 9. Resulting load cycles from the peak history

If there is a large number of counted load cycles, it is practical to group them into e.g. 1000 amplitude classes and accumulate them for a better overview. In this case, the amplitude is defined as the half of the peak-to-peak distance of a load cycle. Those grouped and accumulated load cycles are denoted as load collectives, and the latter is the main result quantity of the turbulence load calculation.

4 REFERENCE MASS AND FLIGHT CONDITIONS

To derive the reference mass of the aircraft, the following points are considered:

- For the mass calculation, the initial state is the operating empty mass configuration.
- The payload should be heavy to bring the aircraft close to the maximum zero-fuel mass to evoke high cut loads at the wing.
- Subsequently, fuel masses are added until the aircraft reaches the maximum take-off mass. Furthermore, the amount of block fuel is estimated as the difference of the actual take-off mass and the maximum landing mass. The fueling sequence is outer tank, inner tank, center tank, and the defueling sequence is center tank, inner tank, outer tank. In other words, the fuel masses should be as far from the aircraft's symmetry plane as possible.

Table 2 lists an overview of the considered masses.

Table 2. Considered masses in the simulation

Parameter	**Value**
Zero-fuel mass	71100 kg
Take-off fuel	14900 kg
Take-off mass	86000 kg
Block fuel	11200 kg
Landing mass	74800 kg

The cruise conditions for the turbulence load calculations are derived as follows:

- For the normal cruise condition, it is assumed that approx. half of the trip fuel has been consumed, the Mach number is 0.78 and the altitude is 35000 ft (FL350, 10668 m).
- For the cruise conditions with varied altitudes, changes in the latter by –4000 ft, –2000 ft and +2000 ft (–1219 m, –610 m and +610 m) are considered based on [3]. At this point, it is considered to be more practical to keep the calibrated airspeed constant as in the normal cruise condition – as opposed to keeping the Mach number or the equivalent airspeed constant. This is because a constant Mach number would lead to varied dynamic pressures, thus varied lift coefficients which are not desirable in transonic conditions. Furthermore, equivalent airspeed is not as simple to measure as calibrated airspeed.
- At the increased altitude of 37000 ft, the true airspeed is higher and the Mach number rises to 0.813. The latter is still below the maximum operating Mach number of 0.82 and is thus feasible.
- For each cruise condition, a turbulence intensity corresponding with a probability of exceedance of 10^{-3} is selected, see Figure 4.

Table 3 lists an overview of the simulation parameters.

Table 3. Overview of the simulation parameters

Flight condition / label	Parameter	Value
Reduced altitude 2 / FL310	Altitude	9449 m (FL310)
	Airspeed	216.8 m/s TAS (Mach 0.718)
	Fuel mass	9448 kg
	Turbulence RMS	1.524 m/s (5.0 ft/s) TAS
Reduced altitude 1 / FL330	Altitude	10058 m (FL330)
	Airspeed	223.9 m/s TAS (Mach 0.748)
	Fuel mass	9448 kg
	Turbulence RMS	1.448 m/s (4.75 ft/s) TAS
Normal cruise / FL350	Altitude	10668 m (FL350)
	Airspeed	231.3 m/s TAS (Mach 0.780)
	Fuel mass	9448 kg
	Turbulence RMS	1.372 m/s (4.5 ft/s) TAS
Increased altitude / FL370	Altitude	11278 m (FL370)
	Airspeed	239.9 m/s TAS (Mach 0.813)
	Fuel mass	9448 kg
	Turbulence RMS	1.295 m/s (4.25 ft/s) TAS

5 LOAD RESULTS

The main result quantities for the turbulence loads are load collectives of the wing bending moment (Mx) and torsion moment (My). Figure 10 illustrates the location of two monitoring stations on the starboard wing and the coordinate system, in which the cut loads are evaluated.

Figure 11 shows load collectives of the flight conditions listed in Table 3. Since the true airspeeds among the flight conditions are different, the load collectives are visualized with regard to distance (per 1000 km of flight) instead of time. It is apparent that with increasing altitude, the amplitude of all cut load quantities in the collectives decline consistently, while the shapes are relatively constant. For the bending moment, the amplitude variations between FL310 and FL370 are approx. –14% at both monitoring stations. In the torsion moment, the amplitude variations are ca. –13% (at the root) and –18% (at 55% span). All of those values correlate with the monotonous change in the turbulence RMS between FL310 and FL370 of –18%, see Table 3.

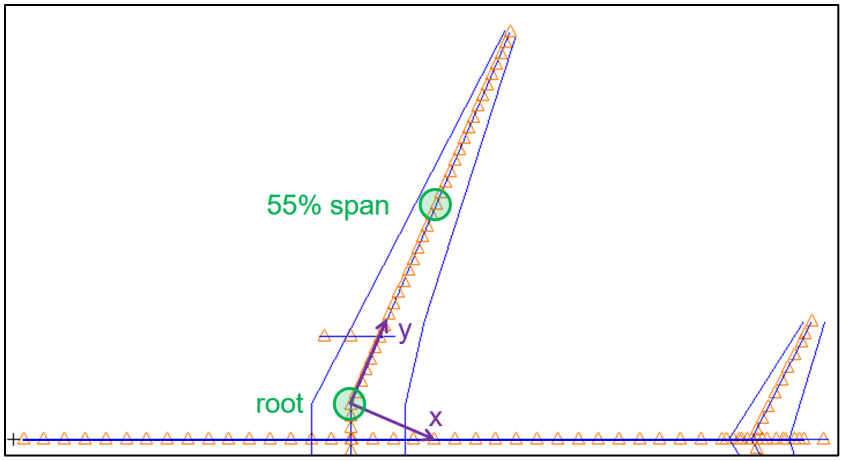

Figure 10. Local coordinate system and monitoring stations on the wing

As a conclusion, the largest fraction of variations in the turbulence loads at the different altitudes is caused by the change in the turbulence RMS itself. The residual variations indicated by the small differences in the shapes of the load collectives emerge from the slightly different dynamic responses of the aircraft at the different altitudes – among others due to the altered true airspeeds and Mach numbers. Those aspects lead to differences in the frequency content of the turbulence, aerodynamic damping as well as flight mechanical derivatives.

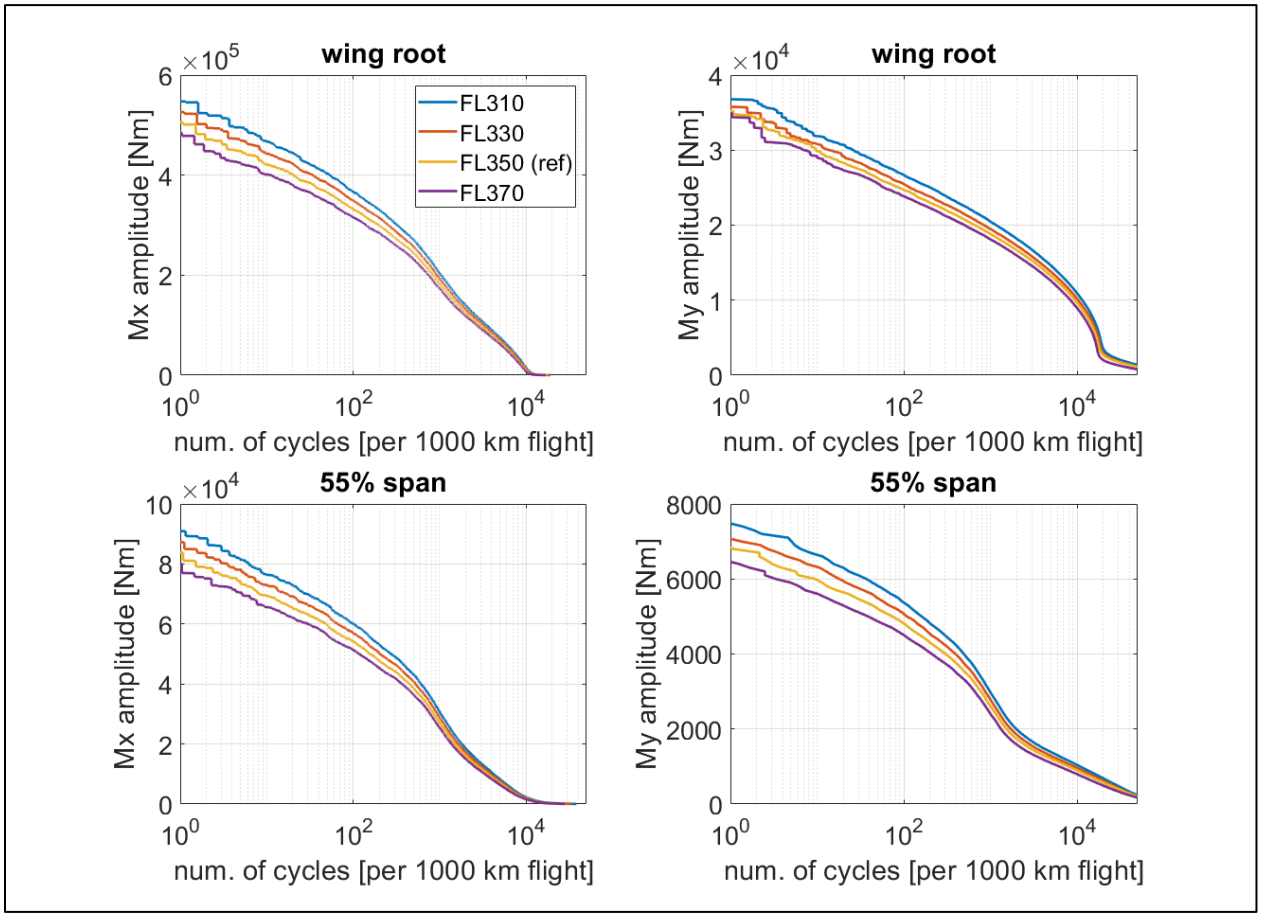

Figure 11. Load collectives of wing bending and torsion moments

Moreover, if the fatigue aspect concerning the variations in cruise altitude – thus turbulence loads – is to be evaluated, it is advisable to consider an entire reference flight mission and observe the strains or stresses at representative locations on the wing box. The flight mission is important because among others ground-air-ground cycles (load cycle between the unloaded wing on the ground and the maximum load factor during the flight) evoke relatively large load amplitudes and might also be a significant contributor to the overall fatigue damage [10]. The strains or stresses are important since they correlate more directly with fatigue compared to cut loads.

Another interesting quantity to observe is the vertical acceleration since it is relevant for the passenger ride comfort. In this case, the vertical acceleration at the fuselage-wing intersection is monitored, and Figure 12 shows the RMS values. Analogous to the cut load amplitudes, the RMS values of the vertical acceleration decline monotonously with increasing altitude (and thus decreasing turbulence RMS). Nevertheless, it is noticeable that the acceleration RMS at the different altitudes deviate slightly from the exact linear behavior with regard to the turbulence RMS. The slight deviations of the acceleration RMS are another indicator for the slightly different aircraft's dynamic responses at the different altitudes.

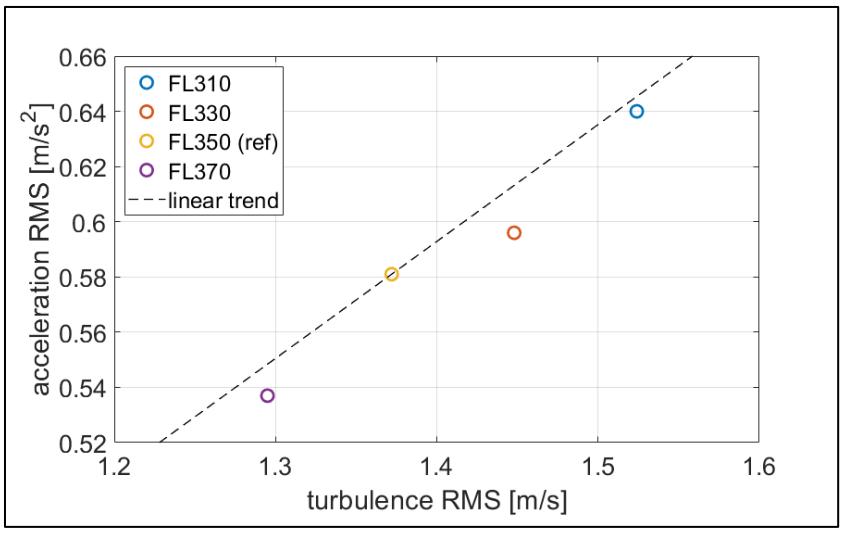

Figure 12. RMS of the vertical acceleration at different altitudes

6 CONCLUSIONS AND OUTLOOK

In total, a method to calculate load collectives due to continuous turbulence has been described and applied on a reference aircraft. On the latter, a variation of the cruise altitude between 31000 ft and 37000 ft (9449 m and 11278 m) has been simulated. In doing so, the calibrated airspeed has been kept constant as in the reference condition and moderate turbulence intensities have been considered. In the resulting turbulence load collectives on the wing, it is apparent that with increasing altitude, the load amplitudes decline monotonously. The same trend is also apparent in the vertical accelerations: with increasing altitude, the root mean square of the vertical acceleration declines monotonously. The largest fraction of the load reduction is caused by the decreasing turbulence intensities at higher altitudes. The residual variations in the loads emerge through the slightly different dynamic responses of the aircraft at the different altitudes.

For the future, if the fatigue aspect related to the cruise altitude variation is to be considered, an evaluation of an entire reference flight mission is advisable to gain a broader overview of the load conditions which might be relevant for fatigue. Besides, it is recommended to monitor stresses or strains at representative locations on the wing box since they correlate directly to fatigue, as opposed to cut loads. Moreover, gust load alleviation functions can also be considered, and their effect on the turbulence loads as well as vertical accelerations can be evaluated. Furthermore, if more information about the aircraft's operational flexibility concerning the cruise altitude variation is available, the parameter space of the turbulence load calculations can be adjusted accordingly.

ACKNOWLEDGMENTS

The authors thank the Federal Ministry for Economic Affairs and Climate Action (Bundesministerium für Wirtschaft und Klimaschutz - BMWK) for the funding as part of LuFo VI-3 in the project AirTiMe.

REFERENCES

[1] M. Bickel, "Climate Impact of Contrail Cirrus," Dissertation, Ludwig-Maximilians-Universität, 2023.

[2] D.S. Lee, D.W. Fahey, A. Skowron, M.R. Allen, U. Burkhardt, Q. Chen, S.J. Doherty, S. Freeman, P.M. Forster, J. Fuglestvedt, A. Gettelman, R.R. De Leon, L.L. Lim, M.T. Lund, R.J. Millar, B. Owen, J.E. Penner, G. Pitari, M.J. Prather, R. Sausen, L.J. Wilcox," The contribution of global aviation to anthropogenic climate forcing for 2000 to 2018," Atmospheric Environment, Vol. 244 (2021).

[3] C. Fichter, S. Marquart, R. Sausen, D.S. Lee, „The impact of cruise altitude on contrails and related radiative forcing," Meteorologische Zeitschrift, Vol. 14 No. 4 (2005).

[4] G. Rädel, K.P. Shine, „Radiative forcing by persistent contrails and its dependence on cruise altitudes," Journal of Geophysical Research, Vol. 113 (2008).

[5] US Department of Defense, "MIL-STD-1797A - Flying Qualities of Piloted Aircraft Notice 3," Technical Report, 2004.

[6] DLR Institute of Aerodynamics and Flow Technology, "Virtual design environment for real, efficient engineering," [Online]. Available: https://www.dlr.de/de/as/forschung-transfer/projekte/virenfrei. [Accessed 21 May 2024].

[7] T. Klimmek, M. Schulze, M. Abu-Zurayk, C. Ilic, A. Merle, "cpacs-MONA – An independent and in high fidelity based MDO tasks integrated process for the structural and aeroelastic design for aircraft configurations," in: International Forum on Aeroelasticity and Structural Dynamics 2019, IFASD 2019, Savannah, GA (USA).

[8] MSC Corporation, "MSC Nastran 2018.2 - Aeroelastic Analysis User's Guide," 2018.

[9] J.P. Giesing, T.P. Kálmán, W.P. Rodden, "Subsonic Steady and Oscillatory Aerodynamics for Multiple Interfering Wings and Bodies," Journal of Aircraft, Vol. 9 No. 10 (1972).

[10] V. Handojo, “Contribution to Load Alleviation in Aircraft Predesign and Its Influence on Structural Mass and Fatigue,” Dissertation, Technische Universität Berlin, Berlin, 2021. https://elib.dlr.de/139558/.

[11] European Aviation Safety Agency, “CS25 - Certification Specifications and Acceptable Means of Compliance for Large Aeroplanes - Amendment 27.” 2021.

[12] H. G. Natke, Einführung in Theorie und Praxis der Zeitreihen- und Modalanalyse. Braunschweig: Friedr. Vieweg und Sohn, 1983.

[13] A. Nieslony, “Rainflow Counting Algorithm,” Rainflow Counting Algorithm – File Exchange - MATLAB Central, 2010. [Online]. Available: https://de.mathworks.com/matlabcentral/fileexchange/3026-rainflow-counting-algorithm. [Accessed: 12-Mar-2024].

COPYRIGHT STATEMENT